

ARTICLE

<https://doi.org/10.1038/s42005-018-0098-0>

OPEN

Switching excitonic recombination and carrier trapping in cesium lead halide perovskites by air

Yue Wang ^{1,2}, Yinjuan Ren³, Shengli Zhang¹, Jianfeng Wu^{4,5}, Jizhong Song¹, Xiaoming Li¹, Jiayue Xu⁶, Chong Haur Sow⁴, Haibo Zeng ¹ & Handong Sun ^{2,7,8}

All-inorganic cesium lead halide perovskites have been emerging as the promising semiconductor materials for next-generation optoelectronics. However, the fundamental question of how the environmental atmosphere affects their photophysical properties, which is closely related to the practical applications, remains elusive. Here, we report the dynamic switching between radiative exciton recombination and non-radiative carrier trapping in CsPbBr₃ by controlling the atmospheric conditions. Specifically, we show that the photoluminescence (PL) intensity from the CsPbBr₃ crystals can be boosted by ~60 times by changing the surrounding from vacuum to air. Based on the comprehensive optical characterization, near-ambient pressure X-ray photoelectron spectroscopy (NAP-XPS) as well as density functional theory (DFT) calculations, we unravel that the physisorption of oxygen molecules, which repairs the trap states by passivating the PL-quenching bromine vacancies, is accountable for the enhanced PL in air. These results are helpful for better understanding the optical properties of all-inorganic perovskites.

¹MIT Key Laboratory of Advanced Display Materials and Devices, Institute of Optoelectronics & Nanomaterials, College of Materials Science and Engineering, Nanjing University of Science and Technology, Nanjing 210094, China. ²Division of Physics and Applied Physics, School of Physical and Mathematical Sciences, Nanyang Technological University, Singapore 637371, Singapore. ³Department of Chemistry, National University of Singapore, 3 Science Drive 3, Singapore 117543, Singapore. ⁴Department of Physics, National University of Singapore, 2 Science Drive 3, Singapore 117542, Singapore. ⁵Department of Electrical and Computer Engineering, National University of Singapore, 4 Engineering Drive 3, Singapore 117576, Singapore. ⁶Institute of Crystal Growth, School of Materials Science and Engineering, Shanghai Institute of Technology, Shanghai 201418, China. ⁷Centre for Disruptive Photonic Technologies (CDPT), Nanyang Technological University, Singapore, 637371, Singapore. ⁸MajuLab, CNRS-UCA-SU-NUS-NTU International Joint Research Unit, Singapore 117543, Singapore. Correspondence and requests for materials should be addressed to H.Z. (email: zeng.haibo@njust.edu.cn) or to H.S. (email: hdsun@ntu.edu.sg)

All-inorganic cesium lead halide perovskites (ILHPs) have been attracting intense interest by virtue of their intriguing potential in photovoltaics, nuclear radiation detectors, light-emitting diodes (LEDs), and lasers, promising for the development of next-generation optoelectronics^{1–5}. Until now, solar cells based on CsPbI₃ have reached 10.77% in power conversion efficiency and the CsPbBr₃-based LEDs have manifested a high external quantum efficiency of up to 10.4%^{1,6,7}. Compared with the organic–inorganic hybrid halide perovskites, the ILHPs feature much enhanced stability against light, moisture, and heat, which is critical for practical applications^{2,5,8}. Moreover, the ILHPs had been demonstrated to show novel and fascinating optical properties, exemplified by the bright triplet-exciton emission and light-driven structural transformations^{9,10}. However, despite of such impressive progresses, the fundamental photophysics of these materials remains largely unexplored, which greatly limits the development of their potential applications^{8,9,11,12}.

It is known that the atmospheric conditions may have considerable impacts on the optoelectronic properties of semiconductor materials and the device performances^{13–16}. Chemisorption and/or physisorption of gaseous molecules on semiconductor crystals could either improve or deteriorate their optical/electronic properties^{14,16–18}. Therefore, understanding the interaction between semiconductors and their environment is essential for the optimization of optoelectronic devices^{18–22}. In the past several years, tremendous research efforts had been devoted to investigating the interaction between organic–inorganic hybrid halide perovskites and their environment, which resulted in a better fundamental understanding and significant improvement of device performances^{15,18,19,23–28}. However, up till now, it much less is known about how the atmospheric condition affects the ILHPs, which may partially account for the currently lagging device efficiency as compared with those made from the hybrid halide perovskites^{6,11,29}. Therefore, deciphering the interaction between ILHPs and air can be crucial for both fundamental research and technological applications, especially for solar cells and LEDs²¹.

In this work, we report the dynamic switching between radiative exciton recombination and carrier trapping on the surface of CsPbBr₃ perovskite crystals by controlling the atmospheric conditions. It is found that the photoluminescence (PL) intensity from the CsPbBr₃ crystals can be boosted by ~60 times by changing the surrounding from vacuum to air. Based on the comprehensive steady-state and dynamic optical characterization, we attribute the enhanced PL in air to the reduced density of trap states associated with the bromine vacancies near the surface region of the crystals. Moreover, in combination of the optical spectroscopic characterization and near-ambient pressure X-ray

photoelectron spectroscopy (NAP-XPS) as well as density functional theory (DFT) calculations, we reveal that the physisorption of oxygen molecules in air could effectively passivate the carrier-trapping bromine vacancies, which contributes to the atmosphere dependent PL behavior. It is noted that the trapping of charge carriers at defects on surfaces is detrimental for the performance of perovskite solar cells and LEDs, our results may provide a new channel for improving the device efficiency based on all-inorganic perovskites, besides highlighting the interesting photophysical property of CsPbBr₃ crystals owing to the interaction with the surrounding atmosphere.

Results

Atmosphere-dependent PL. The CsPbBr₃ perovskite crystals with a high quality were fabricated by the vertical Bridgman technique (see Methods for detailed fabrication process and the representative photos of the samples in Supplementary Fig. 1)^{3,5}. The powder X-ray diffraction (XRD) measurement indicates that the CsPbBr₃ crystals have a well-defined monoclinic perovskite structure (Supplementary Fig. 2), which is consistent with previous results³⁰. Moreover, the high-resolution XRD result reveals the diffraction peak with narrow line-width, demonstrating their highly crystalline nature³.

Figure 1a shows the PL spectra of the CsPbBr₃ crystal in ambient air excited by continuous-wave He-Cd laser (wavelength: 442 nm, power: 1 mW). The sample exhibits a good photostability, manifested by the nearly constant PL intensity under uninterrupted laser irradiation for 1.5 h (Supplementary Fig. 3). To investigate the atmosphere dependence of the PL from the CsPbBr₃ crystal, we monitor the light emission when the chamber is evacuated. Surprisingly, the PL intensity is found to decrease 60 times when the chamber is pumped down to 4.7×10^{-4} Torr (Fig. 1a). The strong PL-quenching phenomenon can be clearly seen even by the naked eyes as shown in Fig. 1a and Supplementary Fig. 4. Figure 1b displays the evolution of the PL intensity from CsPbBr₃ perovskite crystal as the environmental condition exchanges between ambient air and vacuum. It can be seen that the PL intensity decreases rapidly upon air evacuation, then it slows down and finally stabilize at ~1.6% of its initial value. With the refilling of air, the PL intensity increases instantaneously and recovers to the initial state. Such PL switching process can be repeated for many cycles without showing any sign of sample degradation (Supplementary Fig. 5). We further tracked the PL spectrum during the air-vacuum exchange and found that the PL peak position remained unchanged (Fig. 1c) (the representative normalized PL spectra at ambient air and vacuum conditions are displayed as the inset in Fig. 1a, showing the almost identical spectra), implying that the

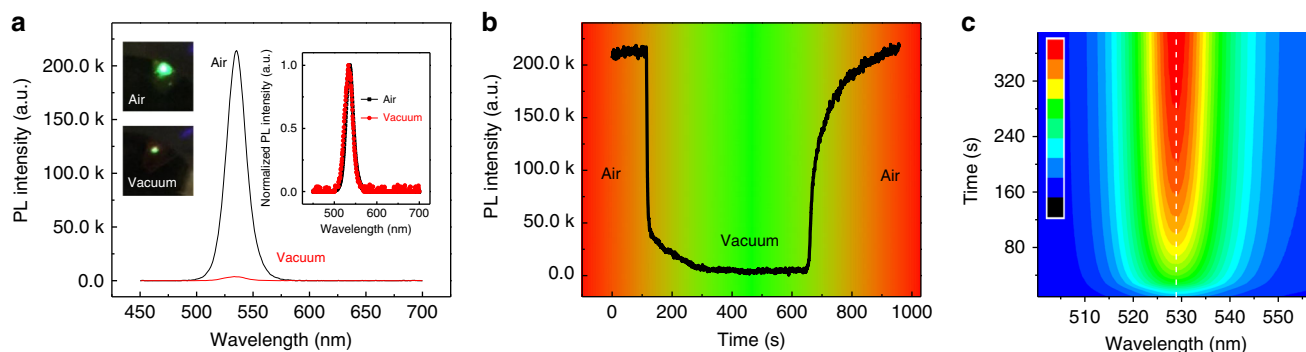


Fig. 1 Photoluminescence (PL) switching in CsPbBr₃. **a** PL spectra of CsPbBr₃. The left inset shows the photograph of CsPbBr₃ in vacuum and air. The right inset shows the normalized PL spectra of CsPbBr₃. **b** Variation in PL intensity of CsPbBr₃ during air-vacuum exchange. **c** Evolution of PL spectrum of CsPbBr₃ with air refilling

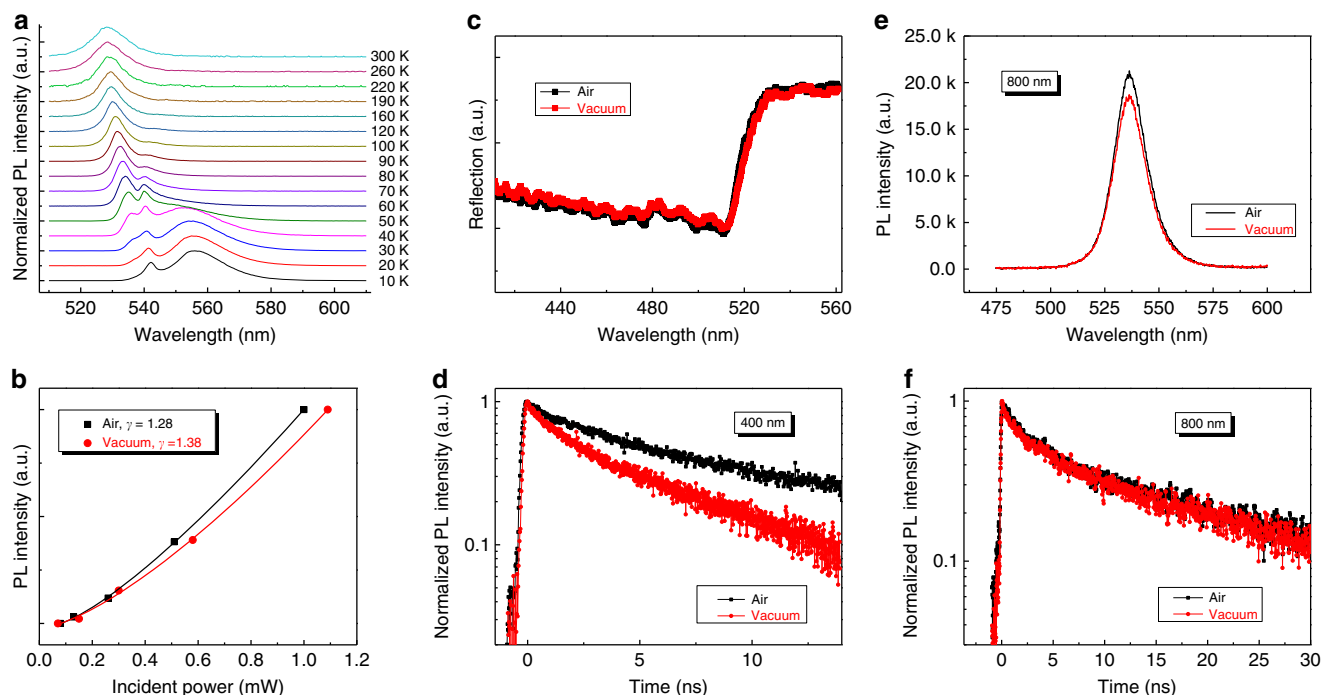


Fig. 2 Optical characterization of CsPbBr₃. **a** Temperature-dependent photoluminescence (PL) spectra of CsPbBr₃. **b** Excitation power-dependent PL intensity from CsPbBr₃. **c** Reflection spectra of CsPbBr₃. **d** PL decay dynamics of CsPbBr₃. **e** Two-photon excited PL spectra of CsPbBr₃. **f** Two-photon excited PL decay dynamics of CsPbBr₃

emission signals under varied atmospheric conditions are originated from the same optical transition. We also have investigated the role of light in the PL switching phenomenon and found that the activation of PL does not require the illumination of the CsPbBr₃ sample. Specially, when the chamber is refilled with air in darkness and then the laser is turned on, the PL sharply achieve and stabilize at the PL maximum rather than monotonic increase of the PL signal (Supplementary Fig. 6). The observation indicates the insignificant role of light in the physisorption of O₂ molecules on the CsPbBr₃ surface, unlike the behavior demonstrated in organic-inorganic perovskites^{26,28}.

To check the generality of the atmosphere dependent PL, we further performed the measurements on the low-temperature solution-grown CsPbBr₃ crystals, which were demonstrated as superior candidates for photon detection^{4,31,32}. As shown in Supplementary Fig. 7, similar PL switching phenomenon was observed, suggesting that the atmosphere dependent PL behavior is quite a general property for CsPbBr₃ perovskite crystals.

Excitonic recombination and carrier trapping. To acquire the mechanism of the atmosphere dependent PL, the origin of the PL from the CsPbBr₃ perovskite crystals has to be understood, which is critical for the further analysis. In general, two possible scenarios may be assumed to account for the boosted PL intensity in air than that in vacuum: (1) The PL originates from the extrinsic radiative defect states, and the defect concentration increases in air. This case has been widely reported in the bulk and nanostructured ZnO semiconductors, where the reduction in “green-band” emission corresponding to the defect-state recombination was observed upon air evacuation^{13,17,33}; (2) If the PL originates from the intrinsic band-to-band or exciton recombination, the reduction of the non-radiative recombination centers in air should be validated. Until now, the PL mechanism from CsPbBr₃ crystals is still controversial. For example, Kanatzidis et al.⁵ claimed that the strongly bound exciton recombination is responsible for the PL from

CsPbBr₃, whereas the above-band-gap emission related to the defect states was reported by Wessels et al.³⁴ To resolve this issue, the temperature- and power-dependent PL measurements were performed in this study as shown in Figs 2a, b, respectively. Supplementary Figure 8 presents the PL spectra of CsPbBr₃ crystal under varied excitation powers at room temperature. The corresponding integrated PL intensity (I_{PL}) as a function of excitation density (I_{EX}) (Fig. 2b) displays a power law dependence: $I_{PL} \propto I_{EX}^{\gamma}$, where γ is the nonlinear component. The γ is derived to be 1.28 and 1.38 for those in the air and vacuum, respectively. This indicates that the PL signals are excitonic in nature (free or bound exciton emission)^{35,36}, consistent with the relatively large exciton binding energy (~40 meV) of CsPbBr₃^{11,37}. Figure 2a shows the temperature-dependent PL spectra of the CsPbBr₃ crystal recorded from 10 K to 300 K. The PL spectrum from CsPbBr₃ crystals at 10 K is dominated by two peaks, locating at 542 nm and 556 nm, respectively. Based on the excitation power-dependent PL measurement (Supplementary Fig. 9), the PL peaks at 542 nm and 556 nm are assigned to the donor-bound exciton (DX) and donor-acceptor pair recombination, respectively (see Supplementary Note 1 for the details of the peak assignments). With the increase of temperature, the peak intensity (542 nm at 10 K) gradually decreases and fades away at ~90 K. Meanwhile, a new emission peak at the shorter wavelength range, corresponding to the free exciton (FX) emission, appears. By tracking the PL evolution with temperature, it is explicitly revealed that the PL of the CsPbBr₃ crystal at room temperature is dominated by the FX emission.

We further recorded the reflection spectra of CsPbBr₃ perovskite crystals in air and vacuum separately (Fig. 2c). It can be seen that the response curves are nearly identical upon the air-vacuum exchange, indicating that there is negligible change in absorption. As such, we speculate that the atmosphere dependent PL in CsPbBr₃ crystals may arise from the reversible trap-density reduction in air as compared with that in vacuum. In other words, air has the effect to passivate the non-radiative trap states. This speculation is further verified by the variation of decay kinetics of

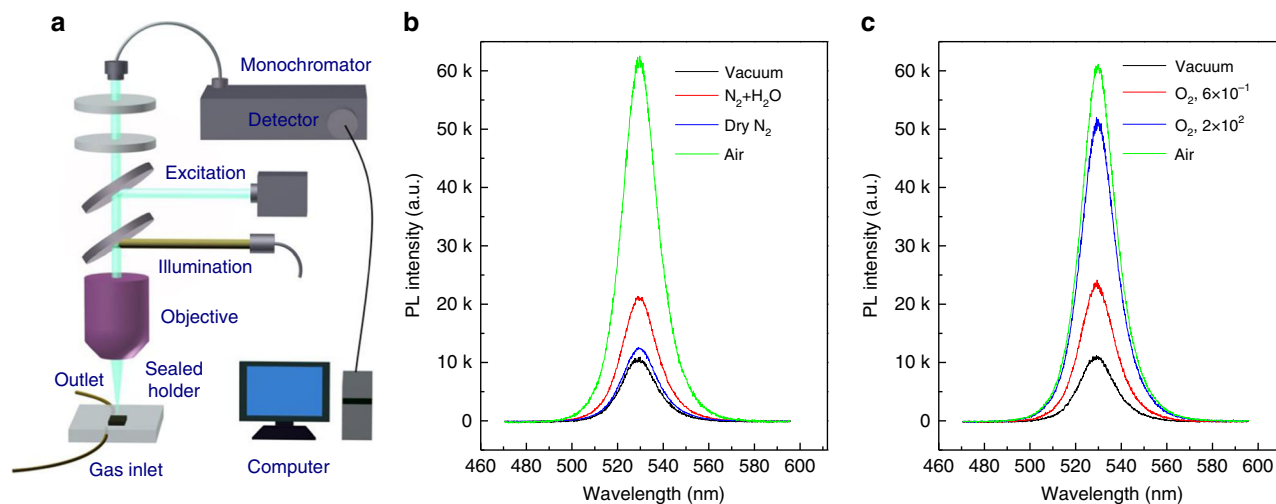


Fig. 3 Photoluminescence (PL) from CsPbBr₃ under different gas atmospheres. **a** Micro-photoluminescence setup. **b** Effects of dry N₂ and moist N₂ on the PL from CsPbBr₃. **c** Effect of O₂ on the PL from CsPbBr₃

CsPbBr₃ crystal during the air-vacuum exchange probed by time-resolved photoluminescence (TRPL). As shown in Fig. 2d, the accelerated decay rate in vacuum than that in air is in agreement with the reduction of trap states by air³⁸, similar to the situation in hybrid perovskite crystals²⁴.

It has been known that the CsPbBr₃ perovskite crystals have a large absorption coefficient of $\sim 1 \times 10^5 \text{ cm}^{-1}$ in the short visible range ($< 500 \text{ nm}$)³, rendering a short penetration depth of only $\sim 100 \text{ nm}$. To selectively explore the interior region of the CsPbBr₃ crystals, the two-photon excitation with much improved penetration capability was employed^{24,39–41}. Figure 2e shows the PL spectra of CsPbBr₃ crystal under excitation wavelength of 800 nm. It is found that the two-photon induced PL are nearly independent on the environmental condition and the corresponding PL dynamics by TRPL are almost the same upon air-vacuum exchange (Fig. 2f), which implies that these atmosphere-sensitive traps lie in the near surface region of the CsPbBr₃ crystals. This is reasonable in terms of twofold aspects: (1) The surfaces directly contact with the external environment and hence facilitate the response to the air-vacuum exchange; (2) It is well-known that the surfaces of semiconductor crystals typically possess much denser defects than the bulk analog⁴¹.

Effect of oxygen molecules. Given that air may interact with the surface and bring about reduced trap density on the surfaces of CsPbBr₃ crystals, it is natural to inquire which gas molecules in air are responsible for the enhanced PL behavior and how. Thus, we monitored the emission variation from CsPbBr₃ crystals under different kinds of gas conditions. Figure 3a presents the schematic illustration of the adopted setup that allows the in situ measurements of PL with varied gas atmosphere (see Methods for more details and the photograph of the setup in Supplementary Fig. 10). It can be seen that there is nearly no change in the PL spectrum when dry N₂ is infiltrated, suggesting that N₂ has negligible impact on the emission of CsPbBr₃ crystal. With the infiltration of moist N₂, the PL intensity shows detectable increase (Fig. 3b). However, the PL intensity under moist N₂ is much weaker than that in air. Notably, the infiltration of O₂ greatly increases the PL intensity and the PL spectrum under O₂ of 2×10^2 Torr almost approaches to that in air (Fig. 3c), indicating that the O₂ dominates the PL enhancement phenomenon in CsPbBr₃ crystals while the moisture only plays a minor role. Moreover, as the PL switching phenomenon is highly reversible, the physisorption rather than chemisorption should be assumed to dictate

the interaction between the oxygen molecules and the CsPbBr₃ crystal^{16,18,42}.

Trap states commonly exist in real semiconductors, which strongly influence or even govern the photophysical properties⁴³. Although the lead halide perovskites are known to be defect tolerant owing to the lacking of bonding-antibonding interaction between the conduction and valence bands⁴⁴, a number of theoretical and experimental investigations have demonstrated the presence of non-negligible defects in them, which effectively trap carriers, giving rise to non-radiative recombination¹⁵. It was reported that Br vacancy (V_{Br}) represents the most common defect in CsPbBr₃ crystals^{43–45}. The previous side-by-side measurements disclosed that the halide-rich circumstance would result in CsPbBr₃ nanocrystals with much higher PL quantum yield than those under halide-deficient counterpart, suggesting that the V_{Br} plays a crucial role in quenching PL^{46–48}. To determine the surface stoichiometry of the sample, we performed the surface-sensitive XPS measurements on the CsPbBr₃ crystal. According to the XPS spectra of Pb 4f and Br 3d obtained under the ultrahigh vacuum (UHV) condition (Figs 4a, b), the atomic ratio of Br/Pb is derived to be ~ 2.6 , indicating that there is indeed Br deficiency in the surface region of the CsPbBr₃ crystal. In fact, anion vacancies are very common in halide semiconductors, especially on the surface of the crystals, owing to its low formation energy^{43,44}. Similar cases were also observed in oxide and sulfide semiconductors, such as ZnO and MoS₂^{13,14,17}. Therefore, it is reasonable to suggest that the enhanced PL from CsPbBr₃ crystals is related to the repair of V_{Br} by physisorption of oxygen molecules.

To confirm the above assumption, we further designed and performed a set of control experiments. It had been widely demonstrated that the wet-chemistry-fabricated CsPbBr₃ nanocrystals possess a Br-rich surface, suggesting that V_{Br} is not significant^{11,46,48}. Accordingly, we carried out the similar optical measurements on the film of CsPbBr₃ nanocrystals, in which the ratio of Br/Pb on the surface was determined to be as high as 3.7 in our previous report⁴⁸. As shown in Figs 4c, d, the pronounced atmosphere dependent PL observed from the CsPbBr₃ perovskite bulk crystals does not happen in wet-chemistry-fabricated CsPbBr₃ nanocrystals, which verifies that the PL switching phenomenon is indeed related to the Br vacancies. Furthermore, it is known that the over-washed CsPbBr₃ nanocrystals will release the dynamic ligands and surface bromine^{49,50}, giving rise to recrystallization into larger crystals and the dramatic decrease

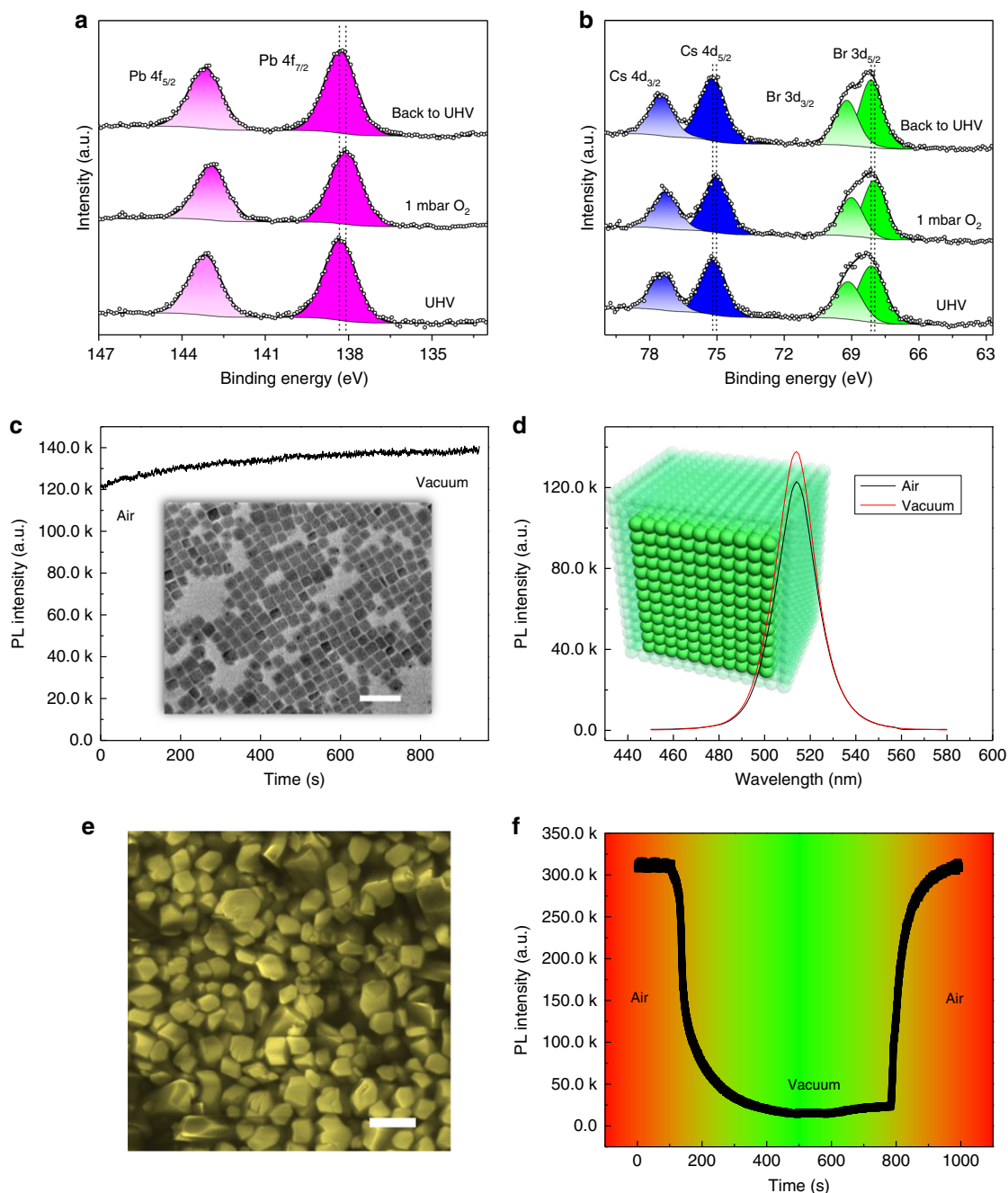


Fig. 4 X-ray photoelectron spectroscopy (XPS) analysis. **a** XPS spectra of Pb 4f core-level in ultrahigh vacuum (UHV) and 1 mbar O_2 . **b** XPS spectra of Br 3d and Cs 4d core-level in UHV and 1 mbar O_2 . **c** Variation in photoluminescence (PL) intensity of colloidal $CsPbBr_3$ nanocrystals. The inset shows the transmission electron microscope (TEM) image. Scale bar is 50 nm. **d** PL spectra of colloidal $CsPbBr_3$ nanocrystals. The inset shows the schematic illustration of $CsPbBr_3$ nanocrystals. **e** Scanning electron microscopy (SEM) image of $CsPbBr_3$ microcrystals. Scale bar is 2 μm . **f** Variation in PL intensity of $CsPbBr_3$ microcrystals

in PL quantum yield possibly owing to the creation of defects associated with Br vacancies^{49,50}. For a more direct comparison, we washed the $CsPbBr_3$ nanocrystals over six times by the normal washing process⁴⁹. Figure 4e shows the scanning electron microscopy image of the obtained $CsPbBr_3$ microcrystals after over-washing the perovskite nanocrystals and the corresponding XPS spectra from these $CsPbBr_3$ microcrystals manifests the Br-deficient surface with a Br/Pb ratio of ~ 2.7 (Supplementary Fig. 11), supporting that bromine in the surface region was removed during the washing process. Notably, when the PL measurement was performed on these over-washed $CsPbBr_3$

microcrystals upon air-vacuum exchange, the PL switching phenomenon was observed again (Fig. 4f), further confirming that the atmosphere dependent PL is related to the passivation of the V_{Br} by oxygen physisorption.

Moreover, we exploited the in-operando NAP-XPS technique to probe the interaction between the oxygen molecules and $CsPbBr_3$ crystals. The bottom spectra in Figs 4a, b present the core levels of Pb 4f, Br 3d, and Cs 4d measured in UHV (5×10^{-10} mbar) and the corresponding binding energies of Pb 4f_{7/2}, Br 3d_{5/2}, and Cs 4d_{5/2} center at 138.3 eV, 68.2 eV, and 75.3 eV, respectively, in line with the literature data⁵¹. After introducing 1 mbar O_2 into

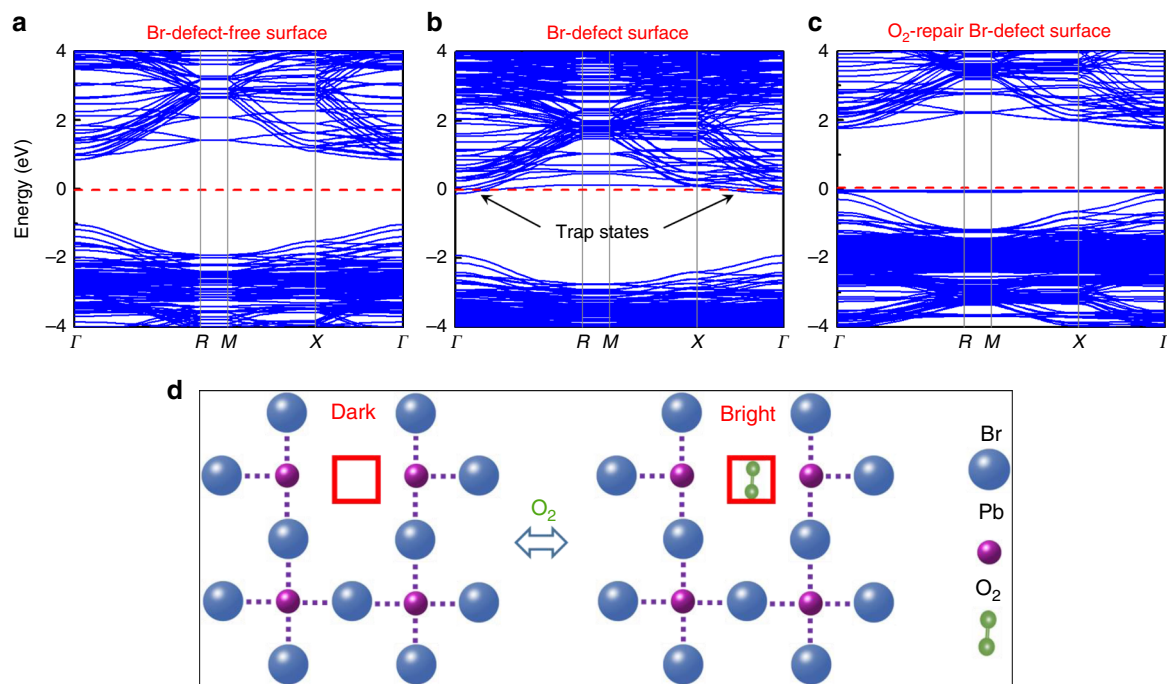


Fig. 5 Density functional theory (DFT) calculations. **a** Band structure of Br-defect-free CsPbBr₃. **b** Band structure of CsPbBr₃ with Br vacancy. **c** Band structure of CsPbBr₃ with Br vacancy and adsorption of oxygen molecule. **d** Schematic illustration of photoluminescence (PL) switching behavior in CsPbBr₃

the NAP cell, the Pb 4f_{7/2} and Pb 4f_{5/2} peaks were found to shift to the lower binding energies by ~ 0.2 eV (Fig. 4a). Similar phenomenon was observed for Br 3d_{3/2}, Br 3d_{5/2}, Cs 4d_{3/2}, and Cs 4d_{5/2} peaks (Fig. 4b). This indicates the occurrence of charge transfer from the CsPbBr₃ crystal to the adsorbed oxygen molecules serving as the electron acceptors⁵², which is in line with our previous work where CsPbBr₃ crystal was determined to be n-type by means of the time-of-flight and Hall measurements³. As the NAP cell goes back to UHV condition (the top row in Figs 4a, b), all the characteristic core-level peaks revert to their initial positions, consistent with the physisorption process.

Density functional theory (DFT) calculations. In order to gain more insights, we performed first-principle DFT simulations to investigate the role of oxygen adsorption onto the (001) surface of CsPbBr₃ crystal in the presence of bromine vacancies (see Fig. 5). We determined that bromine vacancies are the preferred locations for O₂ adsorption compared to the Br-defect-free CsPbBr₃ surface according to the adsorption energy examinations. Similar phenomena had been reported in the organic-inorganic perovskites where the anion vacancies were found to be favorable sites for molecule adsorption^{15,21}. When the O₂ molecules occupy the bromine defect sites, there are noticeable charge redistributions. Further charge analysis suggests that O₂ acts as an electron acceptor with the charge of $-0.8|e|$ from each bromine vacancy of CsPbBr₃, which is consistent with the above NAP-XPS results. In order to further analyze the role of O₂ molecular adsorption, we calculated the band structures of CsPbBr₃ under different conditions. The defect-free CsPbBr₃ has a direct band gap with valence band maximum and conduction band minimum (CBM) both located at the Γ point (Fig. 5a) by using the Perdew-Burke-Ernzerhof (PBE) function^{44,48}. Although, for the CsPbBr₃ surface with bromine vacancies, our calculated results manifest the formation of new shallow energy levels at the bottom of CBM (Fig. 5b). It is noted that the energies from the shallow energy levels to the Fermi level is greater than the thermal energy at room temperature (~ 25 meV), which indicates that these energy

levels could trap charge carriers and give rise to non-radiative recombination¹⁵. Previous calculations by Kang et al. and Shi et al. had given consistent results^{43,44}. When O₂ is adsorbed at the location of the bromine vacancy, the shallow trap states at the bottom of CBM are effectively removed as shown in Fig. 5c. According to the experimental and calculation results, the bromine vacancies act as the shallow donors. These results indicate that adsorption of O₂ can effectively repair the trap states introduced by bromine vacancies, which well explains the observed atmosphere-dependent PL in the CsPbBr₃ crystal.

Discussion

The results presented above demonstrate the interesting dynamic switching of radiative recombination and carrier trapping in CsPbBr₃ which is repeatable and applicable for the crystals grown by both the Bridgman technique and low-temperature solution method. By the comprehensive optical characterization, we attribute the PL origin from the CsPbBr₃ crystal to the free exciton emission and the enhanced PL in air compared to that in vacuum arises from the reduced trap density by O₂ physisorption near the crystal surface. In combination of XPS measurements, control experiments on Br-rich and Br-deficient CsPbBr₃ crystals as well as DFT calculations, we provide the mechanistic insights into the oxygen-induced PL switching behavior. The schematic depiction of O₂-physisorption induced PL switching phenomenon is illustrated in Fig. 5d. Specifically, the bromine vacancies, which are responsible for the PL-quenching in CsPbBr₃ crystals, tend to attract oxygen molecule and the adsorption of O₂ will repair the trap states introduced by V_{Br}, hence leading to the greatly enhanced PL signal. The presence of water vapor also has a positive effect on the PL enhancement. However, compared to the impact of O₂ molecules, the role of H₂O played in PL switching phenomenon is minor. Regarding the PL enhancement by H₂O exposure, there are several possible reasons, such as defect-healing process similar to that seen for O₂ and surface passivation by forming a hydrate layer on the CsPbBr₃ surface. Further research will be required to understand the detailed role

of H₂O on the PL enhancement phenomenon. In the case of polycrystalline CsPbBr₃ films, there exist grain boundaries and noncrystalline domains, which may disturb the intrinsic response of the optical properties to the atmosphere. Nonetheless, the similar surface passivation effect by oxygen physisorption can be anticipated given that the surface is Br-deficient.

Previous research on the interaction between hybrid halide perovskites and their environment had made significant contributions to the fundamental understanding and the optimization of optoelectronic devices. For example, Míguez et al.²⁸ first showed that the oxygen and moisture play an important role in optimizing the light-emitting performance of hybrid perovskites. Fang et al.²⁴ found that the PL of MAPbBr₃ crystals is sensitive to O₂ exposure. They have clearly shown that the PL modulation is related to surface trap state density, and speculated that “a possible reason for the observed PL modulation effect is that the reversible physisorption of O₂ and H₂O acts as a type of molecular gating that donates electron density to the Pb²⁺ cation”²⁴. However, the clarification of the detailed role played by O₂ and H₂O needs more research²³. Especially in view of chemical sensitivity of organic–inorganic halide perovskites to both environmental atmosphere and light illumination, further investigation remains to validate the speculation²⁶. Herein, we aim to investigate the impacts of atmosphere on the photophysics of a new class and technologically important semiconductor CsPbX₃, which is crucial for both fundamental research and practical applications. We demonstrate that O₂ physisorption on CsPbBr₃ surface could modify the electric structure and repair the trap states. Understanding on the photophysics of all-inorganic halide perovskites is still at its early stage. This work does highlight the critical concern about the interaction between the CsPbBr₃ crystals and the environmental atmospheres. These findings help to unify the understanding of the optical properties of the booming CsPbX₃ materials fabricated by different methods and/or measured under different conditions.

Methods

Synthesis of the materials. For the synthesis of CsPbBr₃ perovskite crystals, CsBr (42.6 g) and PbBr₂ (73.4 g) were mixed to obtain the polycrystalline in a silica ampoule. Then, the Bridgman furnace was used to provide the high temperature condition for the growth of the all-inorganic perovskite single crystal. The furnace temperature was optimized to be 627 °C (melting temperature of the perovskite crystal: 567 °C). For the fabrication of CsPbBr₃ nanocrystals, Cs₂CO₃ (0.8 g), oleic acid (2.5 mL), and octadecene (30 mL) were loaded in a 100 mL four-neck flask with degassing at 100 °C for 30 min. Afterwards, the mixture was heated to 150 °C and remains at the temperature for about 0.5 h until all the Cs₂CO₃ being consumed. Then, 1 mL of the Cs-precursor was quickly injected into the hot mixture for reaction. The reaction mixture was cooled by the ice-water bath. Finally, the products were dispersed in toluene. The thin films of the CsPbBr₃ nanocrystals were made by spin-coating method.

Optical characterization. For the atmosphere-dependent optical measurement, the CsPbBr₃ crystal was stored in a sealed chamber, which can be evacuated down to $\sim 4 \times 10^{-4}$ Torr. The sample was excited by a He–Cd laser (wavelength: 442 nm, powder: 1 mW) and the PL was collected through a pair of collimated lens. Then, the signal was dispersed by a 750 mm monochromator and finally detected by a charged coupled device (CCD) or photomultiplier tube. Suitable filters were used in the system. For the temperature-dependent PL, the sample was measured between 10 and 300 K using a helium closed-cycle cryostat. For the time-resolved PL, the sample was pumped at 400 nm by frequency-doubling of the fundamental wavelength (800 nm) and the PL signals were recorded by an Optronix streak camera with an optimized temporal resolution of ~ 50 ps. For the in situ measurements of PL under various gases, the sample was stored in a home-built chamber, which allows the input and output of different kinds of gases at varied pressures, allowing the evacuation down to $\sim 5 \times 10^{-2}$ Torr. The PL signal was collected by a micro-PL setup with $\times 20$ objective and analyzed by a CCD. For the NAP-XPS measurements, the laboratory-based NAP-XPS system, equipped with an Al/Mg twin anode X-ray source and a Specs Phoibos hemispherical energy analyzer, was used. The sample was loaded into the NAP cell for in-operando characterization. Typically, all core-level spectra were referenced to the C 1 s peak at 285.0 eV. The spectrum fitting was performed using CasaXPS, leveraging on the GL30 line shape (G/L ratio of 70/30) and Shirley background subtraction.

DFT calculations. First-principles calculations were performed using density functional theory as implemented in the Vienna ab initio simulation package⁵³. We chose the PBE functional within the generalized gradient approximation to treat the exchange–correlation interaction of electrons⁵⁴. To consider the long-range van der Waals interaction between atomic layers, we adopted the semi-empirical dispersion-corrected D3 scheme proposed by Grimme⁵⁵. O₂ molecules were adsorbed onto an eight layers surface slab of tetragonal CsPbBr₃ containing 80 atoms with a vacuum gap of 20 Å. The energy cutoff for the plane wave basis was chosen to be 500 eV and Brillouin zone integration using the Monkhorst–Pack scheme with $7 \times 7 \times 1$ k-mesh. The convergence criteria of 10^{−5} eV for total energy and a force convergence criterion of 0.001 eV/Å were adopted for self-consistent calculation and geometry optimization, respectively.

Data availability

The data that support the findings of this study are available from the corresponding authors upon reasonable request.

Received: 1 July 2018 Accepted: 13 November 2018

Published online: 17 December 2018

References

- Li, J. et al. 50-fold EQE improvement up to 6.27% of solution-processed all-inorganic perovskite CsPbBr₃ QLEDs via surface ligand density control. *Adv. Mater.* **29**, 1603885 (2017).
- Wang, Y. et al. All-inorganic colloidal perovskite quantum dots: a new class of lasing materials with favorable characteristics. *Adv. Mater.* **27**, 7101–7108 (2015).
- Song, J. et al. Ultralarge all-inorganic perovskite bulk single crystal for high-performance visible–infrared dual-modal photodetectors. *Adv. Opt. Mater.* **5**, 1700157 (2017).
- Dirin, D. N., Cherniukh, I., Yakunin, S., Shynkarenko, Y. & Kovalenko, M. V. Solution-grown CsPbBr₃ perovskite single crystals for photon detection. *Chem. Mater.* **28**, 8470–8474 (2016).
- Stoumpos, C. C. et al. Crystal growth of the perovskite semiconductor CsPbBr₃: a new material for high-energy radiation detection. *Cryst. Growth Des.* **13**, 2722–2727 (2013).
- Swarnkar, A. et al. Quantum dot–induced phase stabilization of α -CsPbI₃ perovskite for high-efficiency photovoltaics. *Science* **354**, 92–95 (2016).
- Zhang, L. et al. Ultra-bright and highly efficient inorganic based perovskite light-emitting diodes. *Nat. Commun.* **8**, 15640 (2017).
- Beal, R. E. et al. Cesium lead halide perovskites with improved stability for tandem solar cells. *J. Phys. Chem. Lett.* **7**, 746–751 (2016).
- Becker, M. A. et al. Bright triplet excitons in caesium lead halide perovskites. *Nature* **553**, 189 (2018).
- Wang, Y. et al. Photon driven transformation of cesium lead halide perovskites from few-monolayer nanoplatelets to bulk phase. *Adv. Mater.* **28**, 10637–10643 (2016).
- Wang, Y. & Sun, H. All-inorganic metal halide perovskite nanostructures: from photophysics to light-emitting applications. *Small Methods* **2**, 1700252 (2018).
- Srimath Kandada, A. R. & Petrozza, A. Photophysics of hybrid lead halide perovskites: the role of microstructure. *Acc. Chem. Res.* **49**, 536–544 (2016).
- Ghosh, M. et al. Role of ambient air on photoluminescence and electrical conductivity of assembly of ZnO nanoparticles. *J. Appl. Phys.* **110**, 054309 (2011).
- Gogoi, P. K. et al. Oxygen passivation mediated tunability of trion and excitons in MoS₂. *Phys. Rev. Lett.* **119**, 077402 (2017).
- Brenes, R., Eames, C., Bulović, V., Islam, M. S. & Stranks, S. D. The impact of atmosphere on the local luminescence properties of metal halide perovskite grains. *Adv. Mater.* **30**, 1706208 (2018).
- Ou, J. Z. et al. Physisorption-based charge transfer in two-dimensional SnS₂ for selective and reversible NO₂ gas sensing. *ACS Nano* **9**, 10313–10323 (2015).
- Liu, K. W., Chen, R., Xing, G. Z., Wu, T. & Sun, H. D. Photoluminescence characteristics of high quality ZnO nanowires and its enhancement by polymer covering. *Appl. Phys. Lett.* **96**, 023111 (2010).
- Tian, Y. et al. Mechanistic insights into perovskite photoluminescence enhancement: light curing with oxygen can boost yield thousandfold. *Phys. Chem. Chem. Phys.* **17**, 24978–24987 (2015).
- Müller, C. et al. Water infiltration in methylammonium lead iodide perovskite: fast and inconspicuous. *Chem. Mater.* **27**, 7835–7841 (2015).
- Tian, Y. et al. Enhanced organo-metal halide perovskite photoluminescence from nanosized defect-free crystallites and emitting sites. *J. Phys. Chem. Lett.* **6**, 4171–4177 (2015).

21. Aristidou, N. et al. Fast oxygen diffusion and iodide defects mediate oxygen-induced degradation of perovskite solar cells. *Nat. Commun.* **8**, 15218 (2017).
22. Stoeckel, M. A. et al. Reversible, fast, and wide-range oxygen sensor based on nanostructured organometal halide perovskite. *Adv. Mater.* **29**, 1702469 (2017).
23. Zhang, H. et al. Reversible air-induced optical and electrical modulation of methylammonium lead bromide (MAPbBr₃) single crystals. *Appl. Phys. Lett.* **111**, 103904 (2017).
24. Fang, H.-H. et al. Ultrahigh sensitivity of methylammonium lead tribromide perovskite single crystals to environmental gases. *Sci. Adv.* **2**, e1600534 (2016).
25. Aristidou, N. et al. The role of oxygen in the degradation of methylammonium lead trihalide perovskite photoactive layers. *Angew. Chem. Int. Ed.* **54**, 8208–8212 (2015).
26. Anaya, M., Galisteo-López, J. F., Calvo, M. E., Espinós, J. P. & Míguez, H. Origin of light-Induced photophysical effects in organic metal halide perovskites in the presence of oxygen. *J. Phys. Chem. Lett.* **9**, 3891–3896 (2018).
27. Brenes, R. et al. Metal halide perovskite polycrystalline films exhibiting properties of single crystals. *Joule* **1**, 155–167 (2017).
28. Galisteo-López, J. F., Anaya, M., Calvo, M. E. & Míguez, H. Environmental effects on the photophysics of organic–inorganic halide perovskites. *J. Phys. Chem. Lett.* **6**, 2200–2205 (2015).
29. Saliba, M. et al. Cesium-containing triple cation perovskite solar cells: improved stability, reproducibility and high efficiency. *Energ. Environ. Sci.* **9**, 1989–1997 (2016).
30. MØller, C. K. Crystal structure and photoconductivity of cesium plumbohalides. *Nature* **182**, 1436 (1958).
31. Ding, J. et al. High detectivity and rapid response in perovskite CsPbBr₃ single-crystal Photodetector. *J. Phys. Chem. C* **121**, 4917–4923 (2017).
32. Rakita, Y. et al. Low-temperature solution-grown CsPbBr₃ single crystals and their characterization. *Cryst. Growth Des.* **16**, 5717–5725 (2016).
33. Gheisi, A. R. et al. O₂ adsorption dependent photoluminescence emission from metal oxide nanoparticles. *Phys. Chem. Chem. Phys.* **16**, 23922–23929 (2014).
34. Sebastian, M. et al. Excitonic emissions and above-band-gap luminescence in the single-crystal perovskite semiconductors CsPbBr₃ and CsPbCl₃. *Phys. Rev. B* **92**, 235210 (2015).
35. Schmidt, T., Lischka, K. & Zulehner, W. Excitation-power dependence of the near-band-edge photoluminescence of semiconductors. *Phys. Rev. B* **45**, 8989–8994 (1992).
36. Chen, R. et al. Exciton localization and optical properties improvement in nanocrystal-embedded ZnO core-shell nanowires. *Nano. Lett.* **13**, 734–739 (2013).
37. Zhang, Q. et al. High-quality whispering-gallery-mode lasing from cesium lead halide perovskite nanoplatelets. *Adv. Funct. Mater.* **26**, 6238–6245 (2016).
38. Leijtens, T. et al. Carrier trapping and recombination: the role of defect physics in enhancing the open circuit voltage of metal halide perovskite solar cells. *Energ. Environ. Sci.* **9**, 3472–3481 (2016).
39. Wang, Y. et al. Nonlinear absorption and low-threshold multiphoton pumped stimulated Emission from all-inorganic perovskite nanocrystals. *Nano. Lett.* **16**, 448–453 (2016).
40. Wang, Y. et al. Stimulated emission and lasing from CdSe/CdS/ZnS core-multi-shell quantum dots by simultaneous three-photon absorption. *Adv. Mater.* **26**, 2954–2961 (2014).
41. Zhong, Y., Wong, K. S., Zhang, W. & Look, D. C. Radiative recombination and ultralong exciton photoluminescence lifetime in GaN freestanding film via two-photon excitation. *Appl. Phys. Lett.* **89**, 022108 (2006).
42. Siedl, N., Gügel, P. & Diwald, O. First combined electron paramagnetic resonance and FT-IR spectroscopic evidence for reversible O₂ adsorption on In₂O_{3-x} nanoparticles. *J. Phys. Chem. C* **117**, 20722–20729 (2013).
43. Shi, H. & Du, M.-H. Shallow halogen vacancies in halide optoelectronic materials. *Phys. Rev. B* **90**, 174103 (2014).
44. Kang, J. & Wang, L.-W. High defect tolerance in lead halide perovskite CsPbBr₃. *J. Phys. Chem. Lett.* **8**, 489–493 (2017).
45. Zeng, Q. et al. Polymer-passivated inorganic cesium lead mixed-halide perovskites for stable and efficient solar cells with high open-circuit voltage over 1.3 V. *Adv. Mater.* **30**, 1705393 (2018).
46. Liu, P. et al. Halide-rich synthesized cesium lead bromide perovskite nanocrystals for light-emitting diodes with improved performance. *Chem. Mater.* **29**, 5168–5173 (2017).
47. Cho, H. et al. Overcoming the electroluminescence efficiency limitations of perovskite light-emitting diodes. *Science* **350**, 1222–1225 (2015).
48. Li, X. et al. CsPbX₃ quantum dots for lighting and displays: room-temperature synthesis, photoluminescence superiorities, underlying origins and white light-emitting diodes. *Adv. Funct. Mater.* **26**, 2435–2445 (2016).
49. Li, X. et al. Healing all-inorganic perovskite films via recyclable dissolution–recrystallization for compact and smooth carrier channels of optoelectronic devices with high stability. *Adv. Funct. Mater.* **26**, 5903–5912 (2016).
50. De Roo, J. et al. Highly dynamic ligand binding and light absorption coefficient of cesium lead bromide perovskite nanocrystals. *ACS Nano* **10**, 2071–2081 (2016).
51. Endres, J. et al. Electronic structure of the CsPbBr₃/polytriarylamine (PTAA) system. *J. Appl. Phys.* **121**, 035304 (2017).
52. Andrä, M. et al. Oxygen partial pressure dependence of surface space charge formation in donor-doped SrTiO₃. *APL Mater.* **5**, 056106 (2017).
53. Kresse, G. & Furthmüller, J. Efficient iterative schemes for ab initio total-energy calculations using a plane-wave basis set. *Phys. Rev. B* **54**, 11169–11186 (1996).
54. Perdew, J. P., Burke, K. & Ernzerhof, M. Generalized gradient approximation made simple. *Phys. Rev. Lett.* **78**, 1396–1396 (1997).
55. Grimme, S., Antony, J., Ehrlich, S. & Krieg, H. A consistent and accurate ab initio parametrization of density functional dispersion correction (DFT-D) for the 94 elements H–Pu. *J. Chem. Phys.* **132**, 154104 (2010).

Acknowledgements

This research is supported by the Singapore Ministry of Education through the Academic Research Fund under Projects MOE2016-T2-1-054, Tier 1-RG105/16, Tier 1-RG92/15, and Tier 1-RG189/17 (S). H.Z. thanks the National Science Fund for Distinguished Young Scholars of China (61604074). J.W. and C.H.S. thank the National Research Foundation (NRF) Competitive Research Programme (CRP) award # NRFCRP13-2014-04.

Author contributions

Y.W., Y.R., and S.Z. contribute equally to this work. The research was initialized by Y.W., Y. R., and H.S. The whole project is supervised by H.S. and H.Z., Y.W., J.W., and C.H.S. conducted spectroscopic experiments and analysis. J.X., X.L., and J.S. fabricated the samples. Y.R. performed the XPS measurements and analysis. S.Z. and H.Z. performed the DFT calculations. All authors get involved in analyzing data, discussing and interpreting detailed results. Y.W. and H. S. drafted the manuscript, and all authors got involved with the revision of the manuscript.

Additional information

Supplementary Information accompanies this paper at <https://doi.org/10.1038/s42005-018-0098-0>.

Competing interests: The authors declare no competing interests.

Reprints and permission information is available online at <http://npg.nature.com/reprintsandpermissions/>

Publisher's note: Springer Nature remains neutral with regard to jurisdictional claims in published maps and institutional affiliations.



Open Access This article is licensed under a Creative Commons Attribution 4.0 International License, which permits use, sharing, adaptation, distribution and reproduction in any medium or format, as long as you give appropriate credit to the original author(s) and the source, provide a link to the Creative Commons license, and indicate if changes were made. The images or other third party material in this article are included in the article's Creative Commons license, unless indicated otherwise in a credit line to the material. If material is not included in the article's Creative Commons license and your intended use is not permitted by statutory regulation or exceeds the permitted use, you will need to obtain permission directly from the copyright holder. To view a copy of this license, visit <http://creativecommons.org/licenses/by/4.0/>.

© The Author(s) 2018